JOURNAL OF AIRCRAFT
Vol. 30, No. 5, Sept.–Oct. 1993

Euler/Experiment Correlations of Sonic Boom Pressure Signatures

Susan E. Cliff*
NASA Ames Research Center, Moffett Field, California 94035
and
Scott D. Thomas†
Sterling Software, Inc., Palo Alto, California 94303

The ability of inviscid computational fluid dynamics (CFD) codes to compute sonic boom pressure signatures is examined using three different codes that solve the Euler equations of fluid flow on structured hexahedral and unstructured tetrahedral grids. The results of these Euler codes were evaluated by comparing the computed pressure signatures with near-field experimental data. The computational pressure signatures were determined at distances of one body length or less below the configuration in the plane of symmetry and extrapolated to experimental distances using the waveform parameter method. The extrapolated CFD pressure signatures gave acceptable correlations with experimental data, provided that fine grids were used between the surface and the spatial location of the pressure signature.

I. Introduction

THE feasibility of a low-boom supersonic transport is again being investigated. A commercial transport is more efficient when supersonic flight is maintained for the entire cruise portion of the mission. However, sonic boom noise may limit the extent of overland supersonic flight over populated areas. A major research effort has begun to design supersonic transport configurations which exhibit acceptable sonic boom characteristics. As part of the design process, computational methods have been developed for analyzing sonic boom characteristics.

Over the past two decades, CFD codes have become capable of computing the flowfield about realistic high-speed civil transport configurations. The simultaneous increase in computational resources is the primary reason that use of these codes has become practical. The use of CFD codes for sonic boom prediction and configuration design offers the potential for making wind-tunnel testing more productive. However, the accuracy of CFD codes for sonic boom prediction needs to be evaluated before application to low-boom design.

The use of Euler flow solvers coupled with extrapolation methods for the computation of sonic boom pressure signatures is a new application of CFD. For instance, Siclari and Darden[1] applied a supersonic Euler code to two low-boom concepts, designed for Mach 2 and Mach 3. The near-field CFD results were extrapolated for comparison with extrapolated wind-tunnel data, corresponding to aircraft at cruise altitude, on and off ground track. The extrapolation method was similar to the one used in the present report. Also, Page and Plotkin[2] calculated the flow about a cone-wing model at Mach 2.01, and extrapolated the near-field pressures on a cylinder around the model for comparison with near-field wind-tunnel data. The approach described below validates the concept of using a planar extrapolation method with an Euler flow solver by comparing extrapolated near-field pressure signatures with experimental data for a range of configurations and flow conditions. The original paper[3] contains additional information, particularly about the grid systems which were used.

II. Approach

Three configurations, shown in Figs. 1–3, were used to validate the computational approach. CFD results were compared with experimental data given in the vertical symmetry plane at Mach numbers ranging from 1.68 to 2.7 and lift coefficients ranging from 0.0 to 0.15 (Table 1). The pressure signatures for the rectangular wing were measured at NASA Langley,[4] those of the cone cylinder and the delta wing/body were measured at NASA Ames.[4,5] These configurations have also been analyzed with a full-potential code[6] and a Navier-Stokes code.[7]

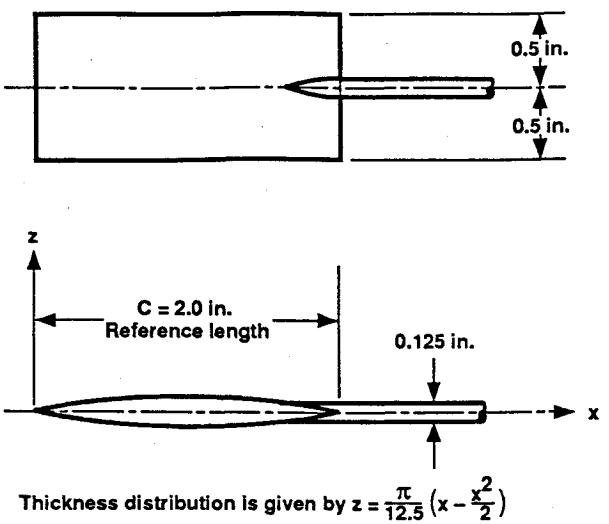

Fig. 1 Low-aspect-ratio rectangular wing.

Received Aug. 14, 1991; presented as Paper 91-3276 at the AIAA 9th Applied Aerodynamics Conference, Baltimore, MD, Sept. 23–25, 1991; revision received July 10, 1992; accepted for publication July 13, 1992.

*Aerospace Engineer, Advanced Aerodynamic Concepts Branch, Aerodynamics Division, MS 227-2. Member AIAA.

†Research Specialist, NASA Ames Division, Federal Systems Group, 1121 San Antonio Road. Senior Member AIAA.

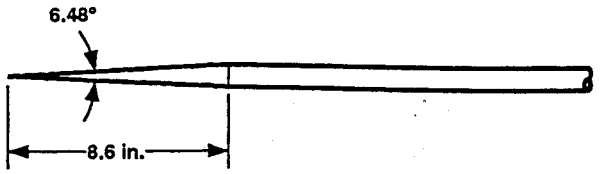

Fig. 2 Cone cylinder.

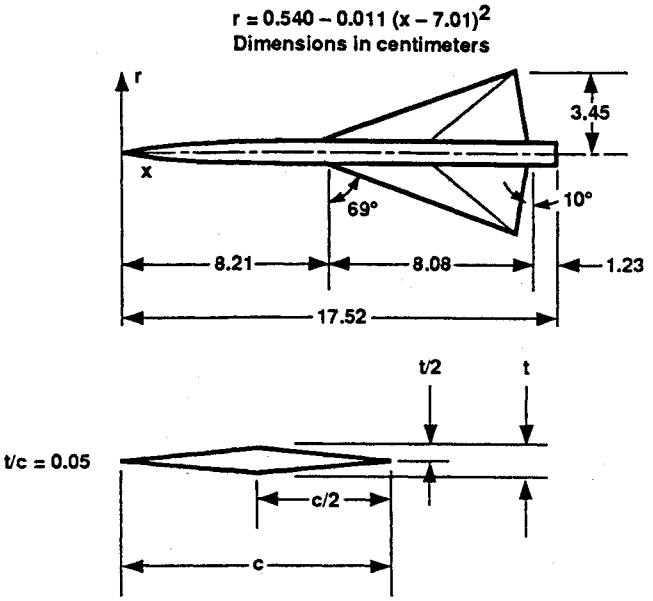

Fig. 3 Delta wing/body.

Table 1 Experimental conditions

Configuration	Mach	C_L	h/l	Salient features
Rectangular wing	2.01	0.0	1.0	N-Wave near and far
Cone cylinder	1.68	0.0	10.0	Approximate finite rise
Delta wing/body	1.68	0.0	3.6	Multiple shocks
	1.68	0.08	3.6	
	1.68	0.15	3.6	
	2.70	0.15	3.1	

The three Euler flow solvers used in the present study are of Jameson and Baker origin (Table 2). The FLO60 code,[8,9] which uses a structured H-H mesh,[10,11] was applied only to the rectangular wing. TEAM, an enhanced version of FLO57,[12] has the ability to use block-structured grids of arbitrary topology without one-to-one abutments.[13] Multiple-zone structured grids for TEAM were generated by the GRIDGEN programs.[14] AIRPLANE models complex configurations using unstructured tetrahedral grids.[15] The AIRPLANE grid generator uses a constrained Delaunay triangulation algorithm.[16,17] The often complicated and time-consuming procedure of blocking and gridding structured multiple-zone grids was eliminated by AIRPLANE, but the surface point distributions required alteration. This was easy to accomplish since the models were analytically defined.

The extrapolation program for this study uses the waveform parameter method of Thomas,[18] which is based on geometric acoustics for the wave amplitude and isentropic theory for the nonlinear waveform distortions and assumes a uniform atmosphere. Experimental pressure signatures for the three models were given at distances ranging from 1.0 to 10.0 body lengths below the model, but obtaining CFD signatures at these distances was difficult with the current methods because of the large computer resources required to maintain dense grids away from the body. Additionally, dissipation inherent in the numerical procedures caused rapid shock strength reduction with increased distance from the configuration. To obtain accurate results, the CFD pressures were sampled at distances ranging from 0.1 to 1.1 body lengths below the configuration. Good correlations were found by selecting a sampling distance for which the strength of the strongest extrapolated shock reached a maximum value at the target experimental distance. Therefore, a balance was found between the decrease in shock strength due to dissipation and the increase due to the three-dimensional effects.

Table 2 Euler flow solvers

Name	Program Description
FLO60	Finite volume, multigrid, vertex-based, automatic H-H grid generation, isolated wing
TEAM	Finite volume, cell-centered, multiblock manual structured grid generation, complete configuration
AIRPLANE	Finite volume, vertex-based, automatic unstructured grid generation, complete configuration

Table 3 Implementation details for CFD codes

Model and code	Computation region	Grid size, points	Central memory, MW	CPU time, h
Rectangular wing				
FLO60	half	1,572,864	62	N.A.
TEAM	quarter	710,701	7	4 Y-MP
AIRPLANE	half	199,383	40	6 Y-MP
Cone cylinder				
TEAM	quarter	372,394	7	1 Y-MP
AIRPLANE	half	166,013	33	8 Cray-2
Delta wing/body				
TEAM	half	1.5×10^6	7	6 Y-MP
AIRPLANE	half	177,281	40	4 Y-MP

Details of the computational grids and typical flow solver requirements on Cray computers for each model are summarized in Table 3. The computer resources required for the extrapolation code were insignificant in comparison. CFD correlations with wind-tunnel data are given for each model in the following sections.

III. Rectangular Wing

Computations with FLO60 using three different grid sizes are compared with experimental pressure signatures (Fig. 4). The computational and experimental pressure signatures are compared at one body length below the wing at $M = 2.01$, $\alpha = 0.0$ deg. Note that the agreement with experiment improves as the number of grid points is increased. The density of the fine grid was insufficient to capture the bow and tail shock at a distance of one body length. When the computational pressures were obtained closer to the model and extrapolated to the experimental distance, good correlation with experiment was obtained. The FLO60 pressure signatures extrapolated from 0.25, 0.5, and 0.75 body lengths to one body length for the fine grid with the sting modeled are shown in Fig. 5. There is a little difference in the bow shock strength when the computational pressures are extrapolated from 0.25 and 0.75 body lengths; both underpredict the bow shock, but the tail shock correlates better with experiment when extrapolated from 0.75. The pressure signature extrapolated from 0.5 predicts the strongest bow shock and correlates well with experiment. The upper and lower limits on h/l for obtaining computational near-field pressure signatures need further study. Dissipation, grid density, wing aspect ratio, lift coefficient, and Mach number are important factors for determining such limits.

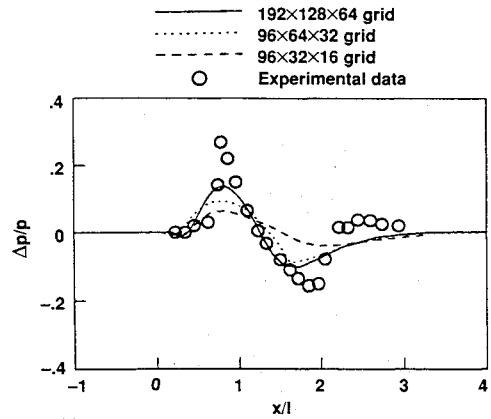

Fig. 4 Effect of grid density for rectangular wing using FLO60, $M = 2.01$, $\alpha = 0$ deg, $h/l = 1.0$.

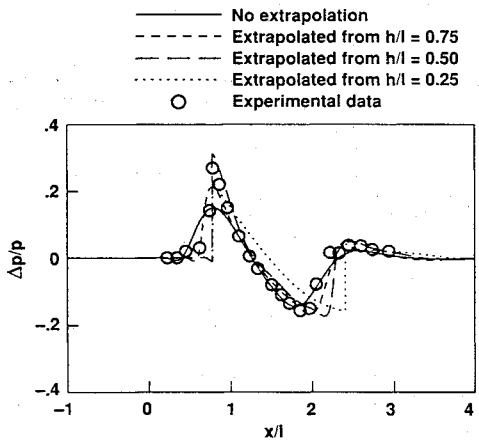

Fig. 5 Effect of extrapolation distance for rectangular wing using FLO60 fine grid, $M = 2.01$, $\alpha = 0$ deg, $h/l = 1.0$.

Pressure signatures were also computed by the TEAM code without extrapolation, using a 10-zone grid. The quarter-space grid was swept 30 deg (approximate Mach angle) from the freestream direction near the wing to maintain grid density and improve shock capture in the flowfield. Dense grids near the bow and tail shocks joined coarse blocks upstream and downstream using 2:1 abutments. The entire block structure of the computational grid including the surface is shown in Fig. 6.

The AIRPLANE code was applied to the rectangular wing using a half-space grid consisting of the triangulated surface and the tetrahedral volume grid. A larger number of grid points was used below the wing than above, to more accurately capture the pressure signatures below the configuration. However, the increased grid density was not sufficient to obtain an accurate signature at one body length.

FLO60, TEAM, and AIRPLANE pressure signatures are compared with experiment in Fig. 7. The computational signatures agree fairly well with the experimental data. FLO60 and AIRPLANE computations included the sting, whereas the TEAM computation did not. The TEAM pressure signature was obtained at one body length from the model, and the FLO60 and AIRPLANE signatures were extrapolated from 0.5 and 0.4 body lengths, respectively, to achieve acceptable correlation with experiment. Note that the bow shock strength is more accurately predicted by TEAM than by FLO60 or AIRPLANE. This may be due to the finer TEAM grid in the region of the bow shock. Note that the rise time of the bow shock decreases when extrapolation is used. The rear shock strength is accurately predicted by TEAM and FLO60, but FLO60 predicts the expansion and tail shock better than TEAM because FLO60 models the sting. The swept and clustered grid used with TEAM enabled it to obtain a more accurate prediction than the AIRPLANE code. The shape and length of the AIRPLANE signature are acceptable, but the bow shock strength is slightly low and the minimum overpressure is more negative than experiment. The less-accurate correlation with AIRPLANE may be due to the rapid decrease in grid density with distance from the surface. In addition, the number of grid points for the tetrahedral mesh is approximately one-tenth the number of hexahedral grid points because of the large computational memory requirements of the unstructured Euler code.

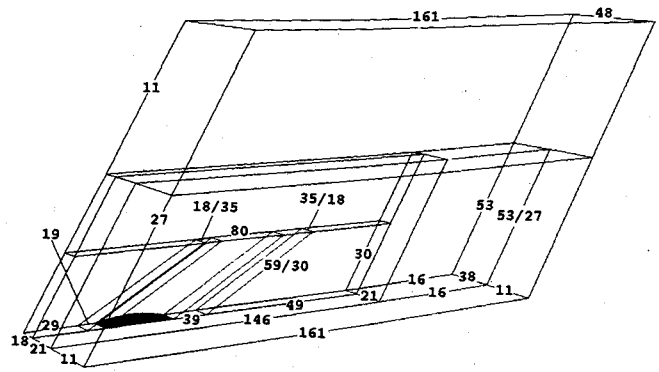

Fig. 6 Rectangular wing TEAM grid.

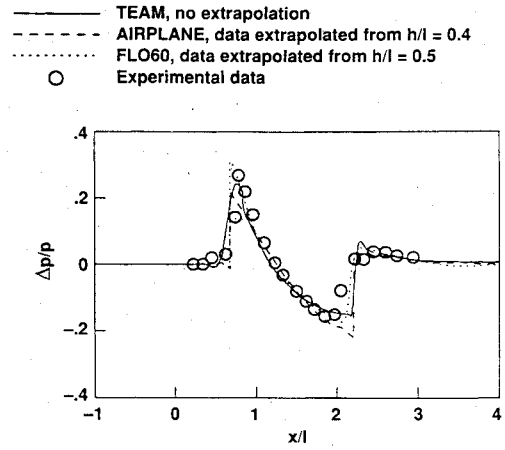

Fig. 7 Code comparison for rectangular wing, $M = 2.01$, $\alpha = 0$ deg, $h/l = 1.0$.

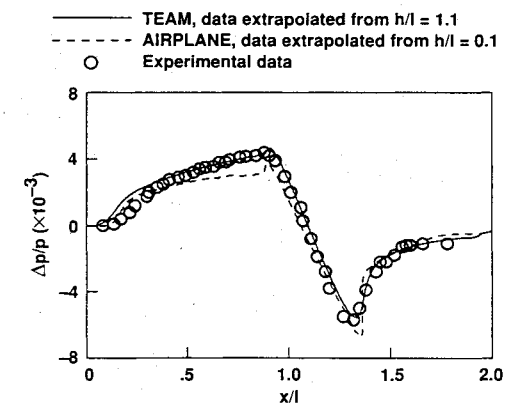

Fig. 8 Pressure signatures for cone cylinder, $M = 1.68$, $\alpha = 0$ deg, $h/l = 10.0$.

IV. Cone Cylinder

TEAM and AIRPLANE were applied to the cone cylinder at $M = 1.68$, $\alpha = 0.0$ deg. The quarter-space grid system used with TEAM for the cone cylinder consisted of four zones swept at the approximate Mach angle, with clustering adapted to the expected solution. AIRPLANE used an asymmetric half-space unstructured grid with more points below the body.

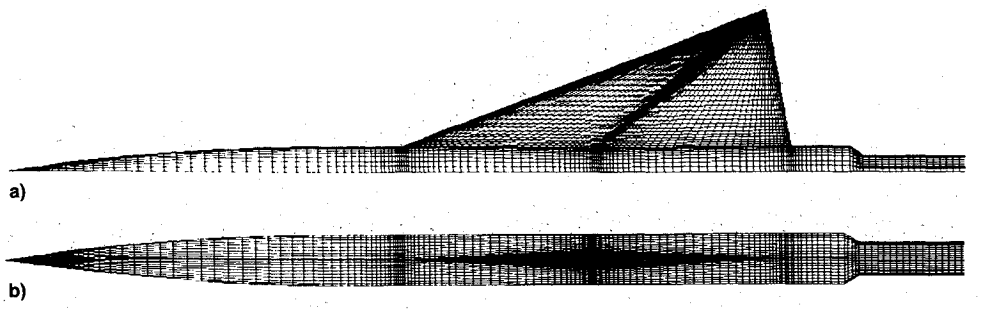

Fig. 9 TEAM multiple-block grid for delta wing/body: a) planform view of surface grid, b) side view of the surface grid.

The TEAM, AIRPLANE, and experimental pressure signatures for the cone cylinder are compared at $h/l = 10.0$ in Fig. 8. The dense TEAM grid allowed acceptable computational pressure signatures at $h/l = 1.1$, whereas the AIRPLANE computational signature was extrapolated from $h/l = 0.1$. The TEAM calculation accurately predicted the finite-rise portion of the signature and the maximum overpressure. The AIRPLANE computation underpredicts the maximum overpressure, but the shape of the signature is good. The slope of the expansion is accurately predicted by both codes. A very small pressure jump at the maximum overpressure is predicted by both codes, but is not physically correct, and is a result of numerical errors. Since the cone cylinder is slender and at zero angle of attack, the computational pressures can be obtained at very small values of h/l without violating the isentropic assumptions of the extrapolation method or missing three-dimensional effects.

V. Delta Wing/Body

The multiple-zone grid used for the TEAM computations consisted of 34 blocks, with 2:1 grid abutments for most far-field blocks to reduce total points. Grid densities above and below the configuration were maintained for one body length downstream to improve shock capture at distances of one-half to one body lengths. The surface grid density used on this configuration was nearly twice the density needed to compute force coefficients,[19] but was retained in order to accurately compute the off-body flowfield. The surface grid was generated using an alternate program.[20] Increased streamwise point density at the leading and trailing edges and at the points of maximum thickness on the upper and lower surfaces of the wing was used to enhance capture of important flowfield phenomena (Fig. 9). The initial grid at the base of the fuselage was open to the far-field boundary to approximately model the sting, which resulted in an underprediction of the rear shock strength at $M = 1.68$, $\alpha = 0.0$ deg. Subsequently, the actual sting was modeled to the downstream boundary and was attached to the base of the fuselage using a short 35-deg ramp.

The AIRPLANE surface definition modeled the junction between the base of the fuselage and the sting with a rearward-facing step (Fig. 10). The sting was closed parabolically to a point at $x/l = 1.57$. The robust AIRPLANE algorithm was able to produce an inviscid solution near the step. A uniform streamwise point distribution sufficed to define the wing at each span station.

TEAM computations were used to establish the angle of attack by matching experimental lift. The reference area used to compute the lift coefficients was 33.1 cm^2, which was found by extrapolating the wing to the centerline along the leading and trailing edges. The AIRPLANE computations for this example are of similar or better accuracy than TEAM when compared with experiment. This is to be expected since an unswept TEAM grid was used for this configuration rather than a swept grid, as was the case for both the rectangular wing and cone cylinder.

The pressure signatures obtained with TEAM and AIRPLANE at $M = 1.68$, $\alpha = 0.0$ deg are shown in Fig. 11. The

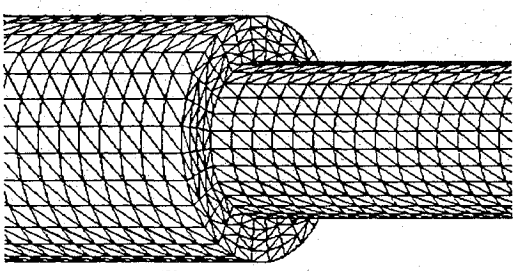

Fig. 10 Expanded view of surface near fuselage/sting intersection. AIRPLANE grid for delta wing/body.

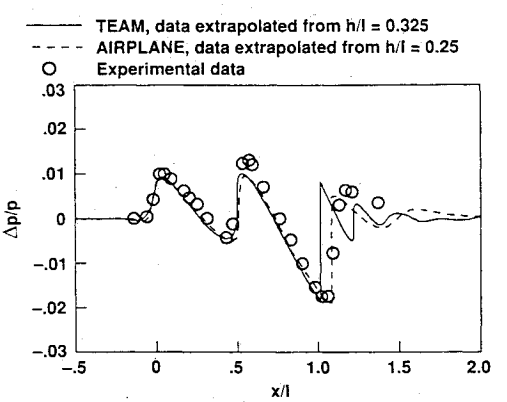

Fig. 11 Experiment/CFD correlation for delta wing/body, $M = 1.68$, $C_L = 0.0$, $h/l = 3.6$.

CFD flowfields were sampled at distances of 0.25 and 0.325 body lengths for AIRPLANE and TEAM, respectively, and were extrapolated to the experimental distance ($h/l = 3.6$). The bow shock is accurately predicted by both codes. The predicted wing shock strengths are slightly low, but the minimum overpressure agrees well with experiment. The correlation clearly would have improved if a larger angle of attack had been used; experimental data usually show some variation of C_N during model travel due to the changing stream angle along the tunnel axis.

Sting modeling effects on the pressure signatures were subsequently studied. The aft portion of the configuration was modeled in two ways using TEAM: 1) with an open base (base of the model extended to the downstream boundary with constant cross-sectional area); and 2) with a 35-deg ramp joining the base of the fuselage to the narrower sting. The ramped sting was expected to cause a larger expansion and recompression shock at the base of the model. The TEAM computations at $\alpha = 1.8$ deg ($C_L = 0.06$) are compared with experiment in Fig. 12. The experimental data ($C_L = 0.08$) are shown for reference only since the computations are at a lower lift coefficient. As expected, the addition of the ramp and sting produced increased tail shock strength. The sting effect at a higher angle of attack ($\alpha = 3.37$) also indicated that the tail shock strength for the ramped sting was stronger

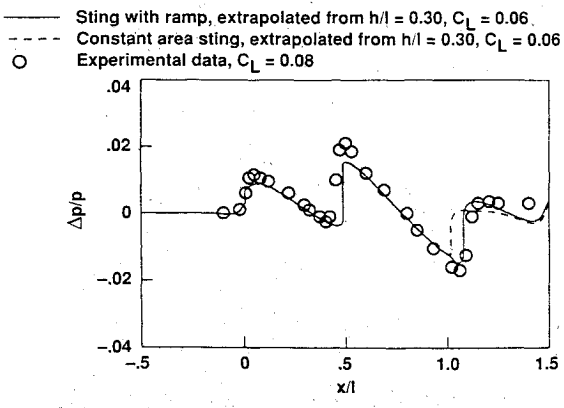

Fig. 12 Effect of shape of fuselage/sting intersection for delta wing/body, $M = 1.68$, TEAM $C_L = 0.06$, $h/l = 3.6$.

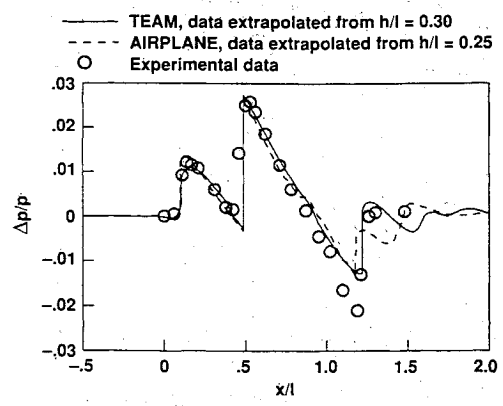

Fig. 14 Experiment/CFD correlation for delta wing/body, $M = 1.68$, $C_L = 0.15$, $h/l = 3.6$.

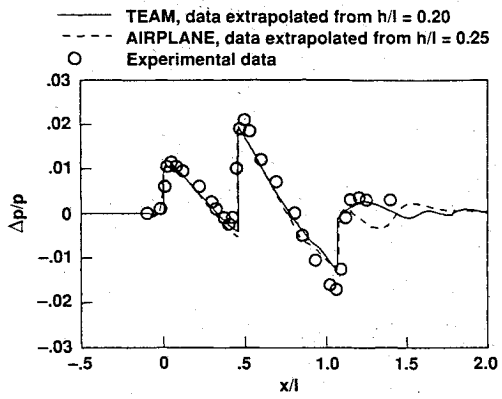

Fig. 13 Experiment/CFD correlation for delta wing/body, $M = 1.68$, $C_L = 0.08$, $h/l = 3.6$.

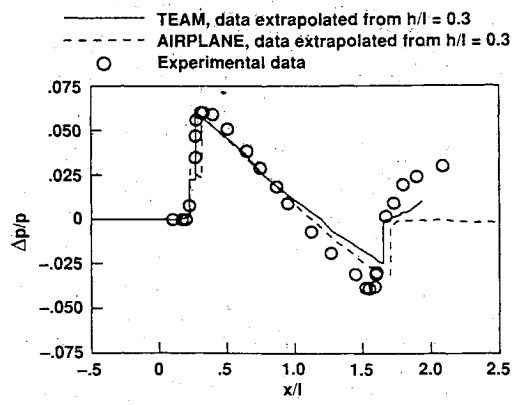

Fig. 15 Experiment/CFD correlation for delta wing/body, $M = 2.70$, $C_L = 0.15$, $h/l = 3.1$.

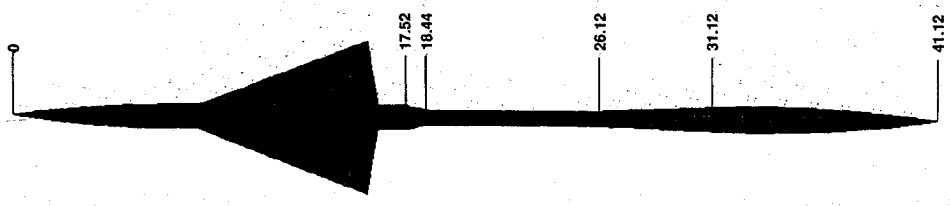

Fig. 16 Planform view of surface with expanding sting and 12-deg ramp to sting, AIRPLANE grid for delta wing/body.

than for the constant-area sting. Subsequent TEAM computations were performed with the ramped sting.

The comparison of experimental pressure signatures with TEAM and AIRPLANE computations at $C_L = 0.08$ ($\alpha = 2.53$ deg), and $h/l = 3.6$ is shown in Fig. 13. The bow and wing shocks agree well with experiment. The tail shock strengths are less than experiment in both cases and are similar (as expected) since the fuselage/sting geometry differences are relatively small. The TEAM computation matches the recovery to freestream conditions better than AIRPLANE because the 35-deg ramp is more realistic than a rearward-facing step for inviscid computations.

The computational signatures at $C_L = 0.15$ and $\alpha = 4.74$ deg are compared with experiment in Fig. 14. The correlation with experiment is good for both codes except the tail shock strength is again less than experiment, possibly because of the unrealistic Euler wake. The increase in bow and wing shock strength with increasing angle of attack is accurately predicted (compare Figs. 13 and 14).

The computational pressure signatures for $M = 2.7$ and $C_L = 0.15$ ($\alpha = 6.52$ deg) are compared with experiment in Fig. 15. The wing and bow shocks have nearly coalesced. The experimental signatures do not have sufficient resolution to show distinct bow and wing shocks. The strength of the combined bow and wing shock correlates well with experiment. However, the tail shock is again underpredicted. The large overshoot of the experimental signature aft of the tail shock may be due to the expanding sting used in the wind-tunnel test, or to shocks from the large angle-of-attack mechanism.

AIRPLANE was used to further investigate the tail shock correlations at positive angles of attack because of the good accuracy obtained by AIRPLANE in the initial computations. In addition, AIRPLANE was chosen for this task because of its automatic grid generation capability which permits different configurations to be meshed with relative ease. The time required to grid a complex configuration using AIRPLANE is nearly an order of magnitude less than that for a structured grid. A 12-deg ramp was used at the base of the fuselage (angle suggested by Whitham[21]), and part of the cone-shaped sting expansion was modeled. A reflected planform view of the surface grid is shown in Fig. 16. An aft view of the fuselage/sting intersection is shown in Fig. 17 (compare with Fig. 10).

Two lifting cases were analyzed: 1) $C_L = 0.08$ ($\alpha = 2.53$ deg); and 2) $C_L = 0.15$ ($\alpha = 4.74$ deg) at $M = 1.68$. AIRPLANE computations with the more accurate sting representation are compared with experiment and with the previous AIRPLANE computations with the rearward-facing step at the base of the fuselage. The effect of modeling the base/sting intersection with a 12-deg ramp followed by a conical sting increased the strength of the tail shock (Figs. 18 and 19). The

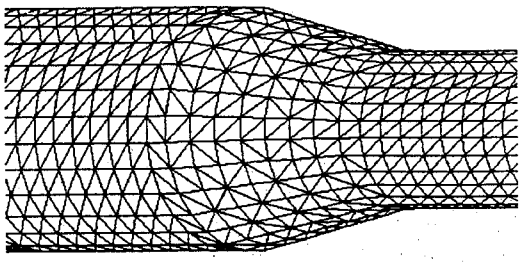

Fig. 17 Expanded view of the surface near fuselage/sting intersection showing 12-deg ramp, AIRPLANE grid for delta wing/body.

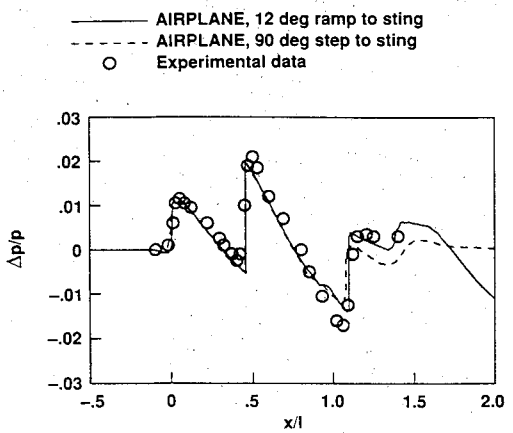

Fig. 18 Effect of fuselage/sting intersection modeling for delta wing/body, $M = 1.68$, $C_L = 0.08$, $h/l = 3.6$, CFD extrapolated from $h/l = 0.25$.

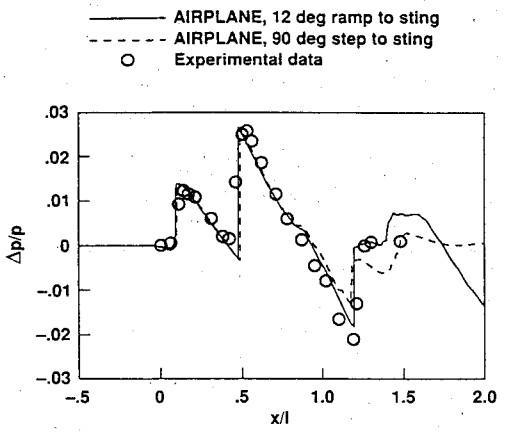

Fig. 19 Effect of fuselage/sting intersection modeling for delta wing/body, $M = 1.68$, $C_L = 0.15$, $h/l = 3.6$, CFD extrapolated from $h/l = 0.3$.

strength and overshoot downstream of the tail shock and the expansion correlate better with experiment when the sting is accurately modeled. The shock from the expanding portion of the sting can be seen in the signatures. The final expansion is due to sting closure.

VI. Concluding Remarks

Euler CFD codes were evaluated by comparing computational and experimental near-field pressure signatures. The results of this study indicated the following.

Euler CFD pressure signatures extrapolated from distances of 1.1 body length or less to experimental distances give acceptable correlations with experimental data, provided that fine grids are used near the surface and downstream of the configuration.

Dissipation in Euler codes used to facilitate convergence causes shocks to dissipate rapidly with increasing distance from the surface. Very fine grids are required even if the data are taken near the model and extrapolated to experimental distances. The quality of the solutions depends on the grid density in the important regions of the flowfield; the topology of the grids is of little importance.

Very good accuracy was obtained by the TEAM code if the grid was clustered in appropriate regions and if the grid was swept at the Mach angle of the freestream flow. If the TEAM grid was not tailored in this manner then comparable or better accuracy was obtained by the unstructured AIRPLANE code.

Mesh generation for the TEAM grids was a time-consuming task which became increasingly longer as the complexity of the configurations increased. In contrast, the mesh generator for the unstructured AIRPLANE code handled all configurations in a largely automatic way and with relatively little user interaction.

Obtaining accurate CFD/experiment correlation for the tail shock of the wing/body was difficult. Improved results were obtained when the sting was modeled and a 12-deg ramp at the base/sting intersection was used. Accurate modeling of the viscous wake might have further improved the tail shock correlations. The shocks from the model-supporting hardware coalesce with the shock waves from the model, especially at higher Mach numbers.

The Euler codes gave acceptable pressure signatures at positive lift coefficients, showing that the computed increase in bow and wing shock strengths with increasing lift were fairly accurate.

References

[1]Siclari, M., and Darden, C., "CFD Predictions of the Near-Field Sonic Boom Environment for Two Low Boom HSCT Configurations," AIAA Paper 91-1631, June 1991.

[2]Page, J. A., and Plotkin, K. J., "An Efficient Method for Incorporating Computational Fluid Dynamics into Sonic Boom Prediction," AIAA Paper 91-3275, Sept. 1991.

[3]Cliff, S. E., and Thomas, S. D., "Euler/Experiment Correlations of Sonic Boom Pressure Signatures," *Proceedings of the AIAA 9th Applied Aerodynamics Conference*, AIAA Paper 91-3276, Washington DC, Sept. 1991, pp. 606–633.

[4]Mendoza, J. P., and Hicks, R. M., "Further Studies of the Extrapolation of Near-Field Overpressure Data," NASA TM-X-2219, March 1971.

[5]Hunton, L. W., Hicks, R. M., and Mendoza, J. P., "Some Effects of Wing Planform on Sonic Boom," NASA TN D-7160, Jan. 1973.

[6]Madson, M. D., "Sonic Boom Predictions for Three Generic Models Using a Solution-Adaptive Full-Potential Code," AIAA Paper 91-3278, Sept. 1991.

[7]Cheung, S. H., Edwards, T. A., and Lawrence, S. L., "Application of CFD to Sonic Boom Near and Mid Flow-Field Prediction," AIAA Paper 90-3999, Oct. 1990.

[8]Jameson, A., "Multigrid Algorithms of Compressible Flow Calculations," *Proceedings of the 2nd European Multigrid Conference*, edited by U. Trottenberg and W. Hackbusch, *Lecture Notes in Mathematics*, Vol. 1228, Springer-Verlag, New York, 1986, pp. 166–201.

[9]Jameson, A., "A Vertex Based Multigrid Algorithm for Three Dimensional Compressible Flow Calculations," *Numerical Methods for Compressible Flows—Finite Difference, Element and Volume Techniques*, edited by T. J. R. Hughes and T. E. Tezduyar, Applied Mechanics Division, American Society of Mechanical Engineers, Vol. 78, Dec. 1986, pp. 45–73.

[10]Baker, T. J., "Mesh Generation by a Sequence of Transformations," *Applied Numerical Mathematics*, Vol. 2, Dec. 1986, pp. 515–528.

[11]Baker, T. J., "Single Block Mesh Generation for a Fuselage Plus Two Lifting Surfaces," *Proceedings of the 3rd International Conference on Numerical Grid Generation in CFD*, edited by A. S. Arcilla, Elsevier, North-Holland, June 1991, pp. 261–272.

[12]Jameson, A., "Transonic Airfoil Calculations Using the Euler Equations," *Proceedings of the IMA Conference on Numerical Methods in Aeronautical Fluid Dynamics*, edited by P. L. Roe, Academic Press, London, 1982, pp. 289–308.

[13]Raj, P., Olling, C. R., Sikora, J. S., Keen, J. M., Singer, S. W., and Brennan, J. E., "Three-Dimensional Euler/Navier-Stokes Aerodynamic Method (TEAM)," Air Force Wright Aeronautical Lab. TR-87-3074, Wright-Patterson AFB, OH, Vols. 1–3, Dec. 1987.

[14]Steinbrenner, J. P., Chawner, J. R., and Fouts, C. L., "The GRIDGEN 3D Multiple Block Grid Generation System," Wright Research and Development Center TR-90-3022, Wright-Patterson AFB, OH, Vol. 1, July 1990.

[15]Jameson, A., and Baker, T. J., "Improvements to the Aircraft Euler Method," AIAA Paper 87-0452, 1987.

[16]Baker, T. J., "Generation of Tetrahedral Meshes Around Complete Aircraft," 2nd International Conf. on Numerical Grid Generation in Computational Fluid Dynamics, NASA and Airforce Office of Scientific Research, Miami Beach, FL, Dec. 1988.

[17]Baker, T. J., "Automatic Mesh Generation for Complex Three-Dimensional Regions Using a Constrained Delaunay Triangulation," *Engineering with Computers*, Vol. 5, Nos. 3 and 4, 1989, pp. 161–175.

[18]Thomas, C. L., "Extrapolation of Sonic Boom Pressure Signatures by the Waveform Parameter Method," NASA TN D-6832, June 1972.

[19]Hicks, R. M., Cliff, S. E., Melton, J. E., Langhi, R. G., Goodsell, A. M., Robertson, D. D., and Moyer, S. A., "Euler and Potential Computational Results for Selected Aerodynamic Configurations," *Applied Computational Aerodynamics*, edited by P. A. Henne, Vol. 125, Progress in Astronautics and Aeronautics, AIAA, Washington, DC, 1990, pp. 263–385.

[20]Melton, J. E., and Langey, R. G., "Surface Grid Generation for Advanced Transport Configurations," *Numerical Grid Generation in Computational Fluid Mechanics '88*, Pineridge Press International, Swansea, Wales, UK, 1988, pp. 751–759.

[21]Whitham, G. B., "The Flow Pattern of a Supersonic Projectile," *Communications on Pure and Applied Mathematics*, Vol. 5, No. 3, 1952, pp. 301–348.